Journal of Computational Physics 228 (2009) 257–265

Contents lists available at ScienceDirect

Journal of Computational Physics

journal homepage: www.elsevier.com/locate/jcp

Short Note

A stability analysis for the spectral volume method on tetrahedral grids

K. Van den Abeele *,[1], G. Ghorbaniasl, M. Parsani, C. Lacor

Vrije Universiteit Brussel, Department of Mechanical Engineering, Fluid Dynamics and Thermodynamics Research Group, Pleinlaan 2, 1050 Brussel, Belgium

ARTICLE INFO

Article history:
Received 18 March 2008
Received in revised form 17 September 2008
Accepted 3 October 2008
Available online 17 October 2008

Keywords:
Spectral volume method
Unstructured tetrahedral grids
Stability

1. Introduction

The spectral volume (SV) method was introduced in 2002 by Wang [1]. Its further development, such as the extension to 2D and 3D and the application to the Euler and Navier–Stokes equations, was reported by Wang et al. [2–5], Liu et al. [6] and Sun et al. [7]. Recently, a more efficient, quadrature-free implementation of the SV method was presented in Harris et al. [8]. A number of high-order SV schemes for triangles and tetrahedrons were defined in Chen [9]. The SV method is related to the discontinuous Galerkin method, see e.g. Cockburn and Shu [10], and the references therein, and to the spectral difference (SD) method, see e.g. Sun et al. [11]. All these methods use piecewise continuous polynomials to represent the solution. Moreover, in Van den Abeele et al. [12], it was shown that in 1D, the SV and SD methods are equivalent.

In Van den Abeele et al. [13] and Van den Abeele and Lacor [14], the stability of the SV method was analyzed for 1D and 2D, respectively. Several SV schemes that have been used in literature were found to suffer from weak instabilities, and stable SV schemes were proposed for 1D and 2D. In the present note, the stability of the SV method on 3D tetrahedral grids is analyzed using the matrix method, see e.g. Hirsch [15]. The second-order scheme and four families of third-order schemes are investigated. Although the second-order scheme is stable, a surprising result is that no stable scheme was found in any of the four families of third-order schemes.

The rest of this note is organized as follows. A brief summary of the SV method is given in Section 2. In Section 3, 3D SV partitions on a tetrahedron are defined, after which the methodology for the stability analysis is explained in Section 4. The results of the stability analysis are then discussed in Section 5 and conclusions are drawn in Section 7.

* Corresponding author. Tel.: +32 26292399; fax: +32 26292880.
E-mail addresses: kvdabeel@vub.ac.be (K. Van den Abeele), krisvda@gmail.com (K. Van den Abeele), ghader.ghorbaniasl@vub.ac.be (G. Ghorbaniasl), mparsani@vub.ac.be (M. Parsani), chris.lacor@vub.ac.be (C. Lacor).
[1] FWO Research Engineer.

doi:10.1016/j.jcp.2008.10.011

2. Spectral volume method

The spectral volume method is used to solve conservation laws (1)

$$\frac{\partial U}{\partial t} + \vec{\nabla} \cdot \vec{F}U = 0. \tag{1}$$

The computational domain V is divided in N^{SV} cells V_i, called spectral volumes, with volume $|V_i|$. Each SV is further subdivided into control volumes (CV) V_{ij}. Integrating (1) over such a CV and applying the Gauss theorem give

$$\frac{\partial \overline{U}_{ij}}{\partial t}|V_{ij}| = -\int_{\partial V_{ij}} \vec{F} \cdot d\vec{s}, \tag{2}$$

where $|V_{ij}|$ is the volume of V_{ij} and $\overline{U}_{ij}$ is the CV average defined by

$$\overline{U}_{ij} \equiv \frac{1}{|V_{ij}|}\int_{V_{ij}} U dV. \tag{3}$$

On a spectral volume V_i, the SV polynomial approximation of the solution is defined

$$U_{V_i} \approx u_{V_i} \equiv \sum_{j=1}^{N^{CV}(p,d)} \overline{U}_{ij}\overline{L}_{ij}. \tag{4}$$

In Eq. (4), $N^{CV}(p,d)$ is the number of CVs in a SV, depending on the desired degree of the polynomial approximation p and the number of spatial dimensions d. The polynomials $\overline{L}_{ij}$ associated to the CVs V_{ij} are defined by

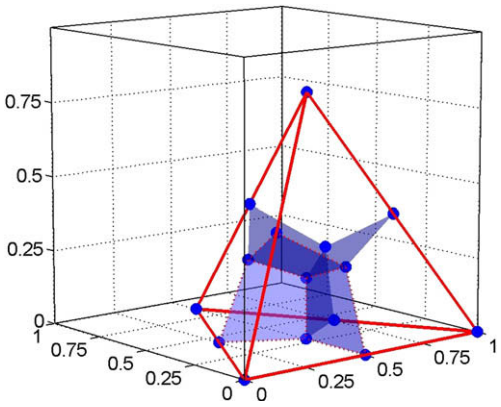

Fig. 1. Second-order 3D SV partition.

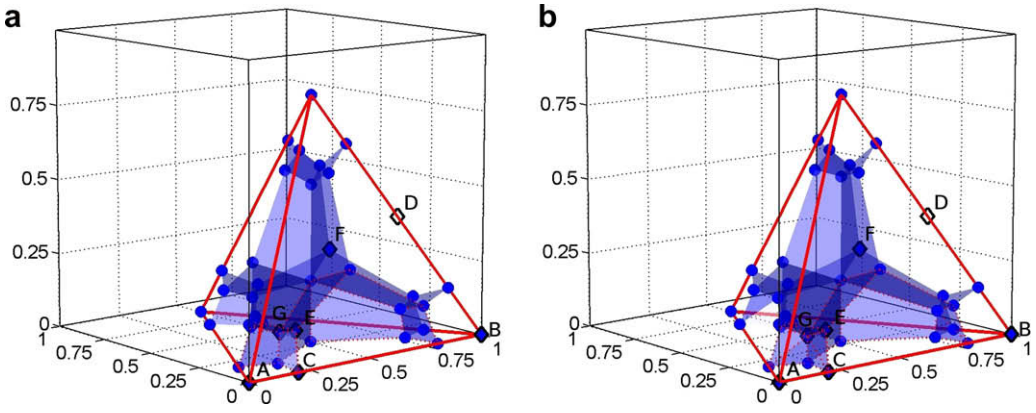

Fig. 2. Two-parameter family (a) and first three-parameter family (b) of partitions for a third-order 3D SV partition.

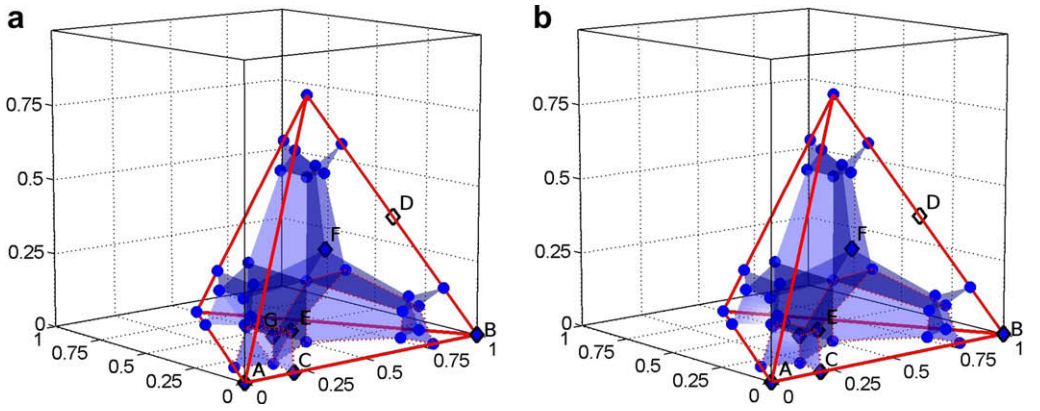

Fig. 3. Second (a) and third (b) three-parameter family of partitions for a third-order 3D SV partition.

$$\frac{1}{|V_{i,j}|}\int_{V_{i,j}} \bar{L}_{i,m}\,dV = \delta_{jm}, \tag{5}$$

where δ_{jm} is the Kronecker delta function. With the polynomial approximation u_{V_i}, the flux integral in (2) can be approximated to order $p+1$, using Gauss quadrature. On the boundary between two SVs however, there are two available values for the flux $\vec{F}$, one from within each SV. Thus on these boundaries a suitable Riemann flux $\vec{F}^R$, for instance the Rusanov flux, must be used. A more elaborate overview of the SV method can be found in [1–4,6,7].

3. 3D spectral volume partitions

The second-order partition is uniquely defined and is plotted in Fig. 1.

The third-order partition is not uniquely defined. Four possible partition families are illustrated in Figs. 2 and 3. In general, three parameters are needed to define a third-order partition. Here, the following parameters are used: $\alpha = |AC|/|AB|$, $\beta = |AE|/|AD|$ and $\gamma = |AG|/|AF|$, where the points A to G are shown in the figures. These are the same parameters that were used in Liu et al. [6]. Their values lie in the following intervals: $\alpha \in]0, 1/2]$, $\beta \in]0, 2/3]$ and $\gamma \in]0, 3/4]$.

The family of partitions in Fig. 2(a) is a simplified case, where it is imposed that the internal faces of the corner CVs are planar. This way, two free parameters remain, namely α and β, with the third parameter γ defined by

$$\gamma = \frac{3\alpha\beta}{4\alpha - \beta}. \tag{6}$$

This is the family of partitions that was considered in Liu et al. [6] and Chen [9]. Notice that for this family, there are further restrictions on the values that α and β can assume, namely $\beta < 4\alpha$ for γ to be greater than zero, and $\beta \leqslant 4\alpha/(4\alpha+1)$ to satisfy $\gamma \leqslant 3/4$. Notice that the second condition is more restrictive than the first.

For the second and the third family of partitions, shown in Figs. 2(b) and 3(a), respectively, all parameters can be chosen freely. The internal faces of the corner CVs are subdivided into two triangles. As can be seen in the figures, the two families

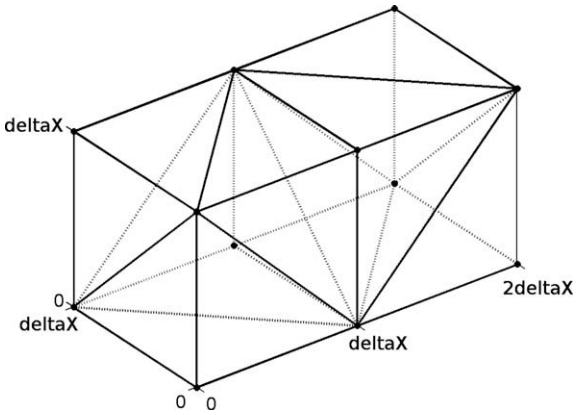

Fig. 4. Generating pattern of the mesh used for the analysis.

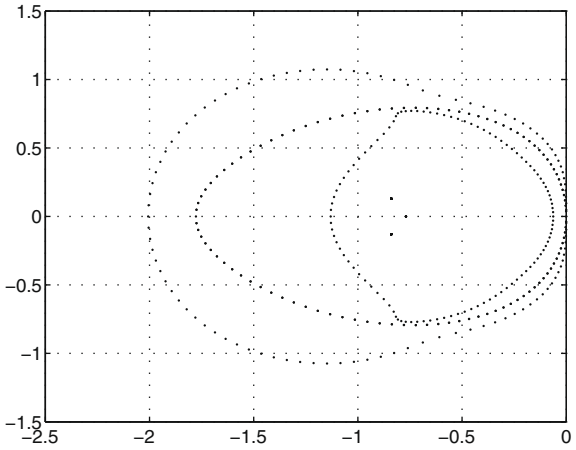

Fig. 5. Distribution of eigenvalues of the matrix M for the second-order 3D SV scheme in the complex plane.

differ in the way these faces are subdivided. For the last family of partitions, shown in Fig. 3(b), the internal faces of the corner CVs are treated as a single bilinear quadrilateral face (no additional edge is introduced).

4. Methodology for stability analysis

The method for the stability analysis used here is the matrix method, as described in Hirsch [15], applied to the 3D linear advection equation

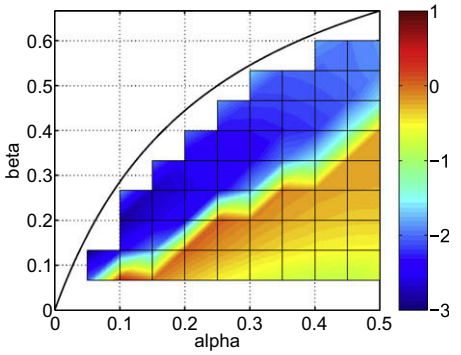

Fig. 6. Logarithm in base ten of maximum real eigenvalue of the matrix M for the first family of third-order partitions, for partition parameters $\alpha = 1/20 + l\frac{1}{20}$ and $\beta = 2/30 + m\frac{2}{30}$, with $l, m = 0, \ldots, 9$.

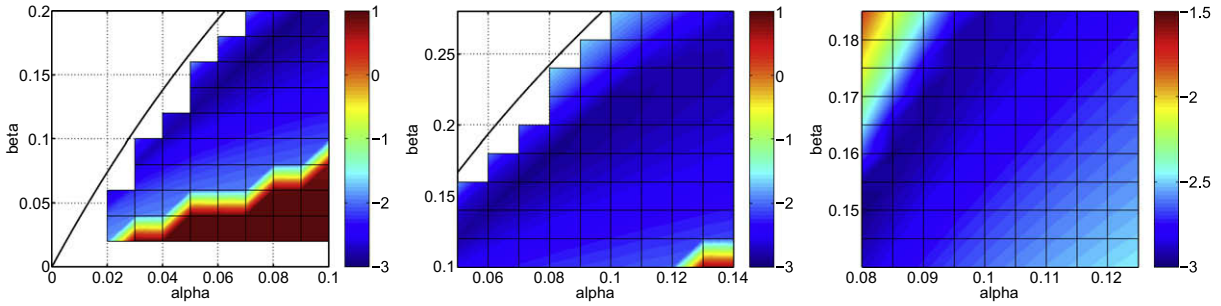

Fig. 7. Logarithm in base ten of maximum real eigenvalue of the stability analysis matrix for the two-parameter family of third-order partitions. Zooms in the (α, β) domain, in zones with small values for the maximum real eigenvalues.

$$\frac{\partial u}{\partial t} + \vec{\nabla} \cdot (\vec{a}u) = 0, \tag{7}$$

where $\vec{a}$ is the propagation speed. This equation is discretized in space with the SV method, on a mesh formed by periodically repeating the generating pattern, shown in Fig. 4, N^{GP} times along the direction with three nodes in the generating pattern, creating a long channel. The mesh then contains $N^{SV} = 10 \times N^{GP}$ cells and $N^{CV,tot} = N^{SV} \times N^{CV}$ CV-averaged solutions.

The cell size Δx is defined by the shortest distance between two nodes in the generating pattern. The propagation speed $\vec{a}$ is directed along the channel axis and the inlet and outlet of the channel are connected, creating a periodic direction. Since $\vec{a}$ is directed along the channel axis, the boundary conditions on the sides of the channel have no influence, because the flux through these faces is zero. The exact solution is then an undamped propagation of the initial solution along the channel.

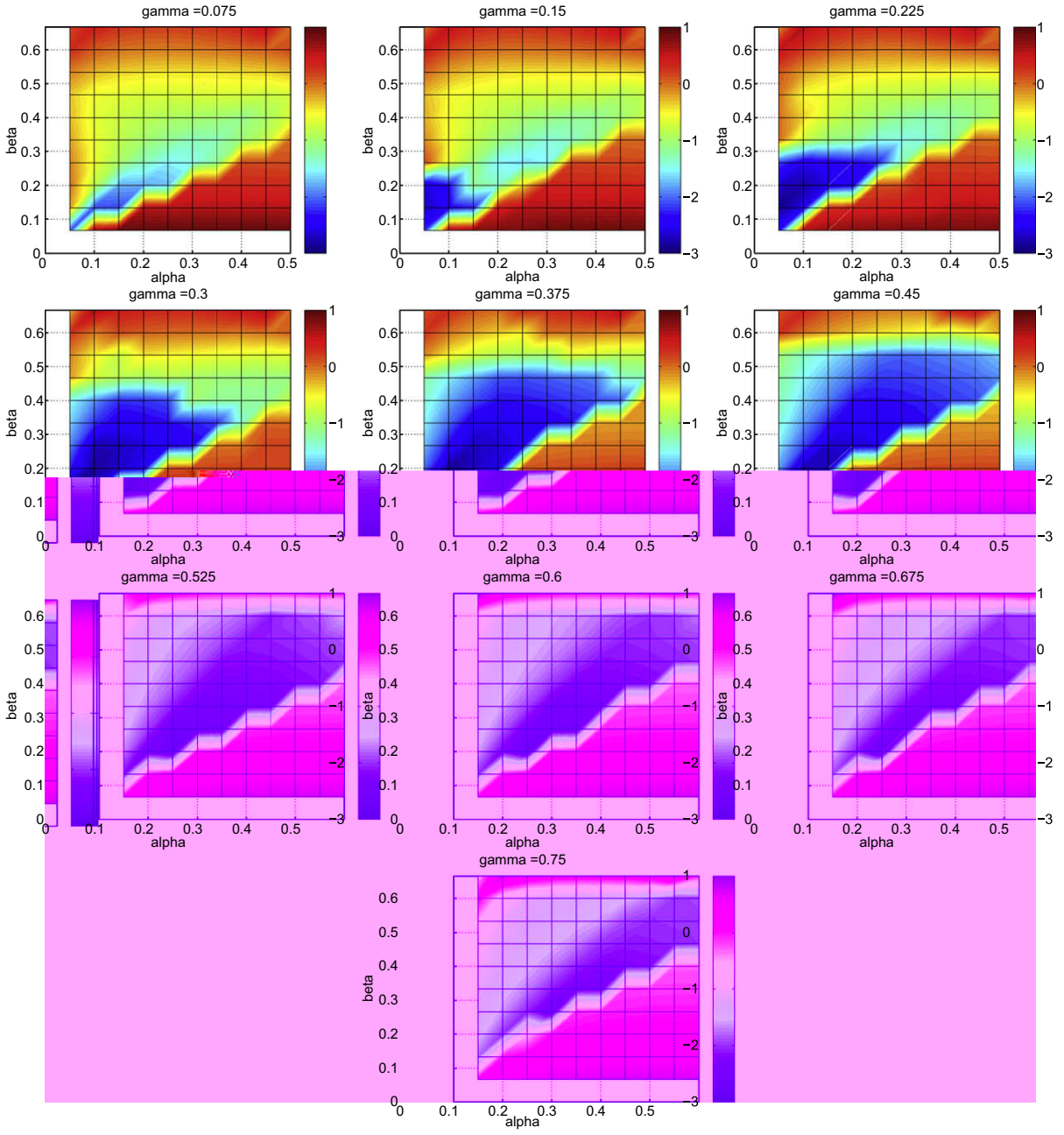

Fig. 8. Logarithm in base ten of maximum real eigenvalue of the matrix **M** for the first three-parameter family of third-order partitions, for partition parameters $\alpha = \frac{1}{20} + l\frac{1}{20}, \beta = \frac{2}{30} + m\frac{2}{30}$ and $\gamma = \frac{3}{40} + n\frac{3}{40}$, with $l, m, n = 0, \ldots, 9$.

This configuration was chosen because it allows to detect weak instabilities in solution modes with a long wavelength with respect to the cell size Δx, which were found to be a problem of many 1D and 2D SV partitions in [13,14].

The problem is non-dimensionalized using

$$[x \quad y \quad z]^\tau = \Delta x[x' \quad y' \quad z']^\tau \quad \text{and} \quad t = \frac{\Delta x}{|\vec{a}|}t'. \tag{8}$$

Eq. (7) then becomes, after spatial discretization and non-dimensionalization,

$$\frac{\partial \overline{\mathbf{U}}}{\partial t'} = \mathbf{M}\overline{\mathbf{U}}, \tag{9}$$

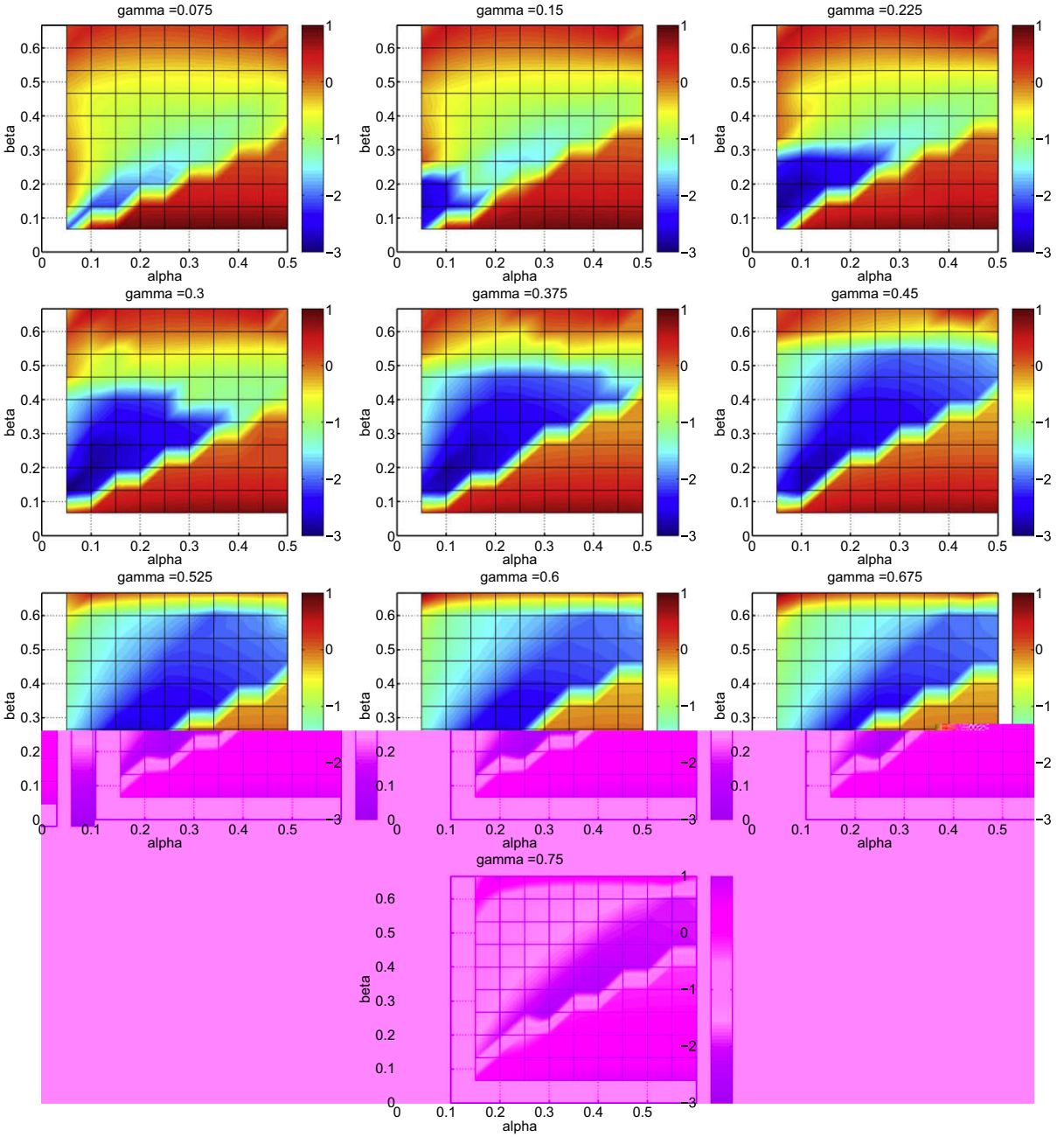

Fig. 9. Logarithm in base ten of maximum real eigenvalue of the matrix **M** for the second three-parameter family of third-order partitions, for partition parameters $\alpha = \frac{1}{20} + l\frac{1}{20}, \beta = \frac{2}{30} + m\frac{2}{30}$ and $\gamma = \frac{3}{40} + n\frac{3}{40}$, with $l, m, n = 0, \ldots, 9$.

where $\overline{\mathbf{U}}$ is a column vector containing all the CV-averaged solutions on the mesh and the matrix $\mathbf{M}$ is a function of the mesh, the scheme and the propagation direction $\vec{1}_a = \vec{a}/|\vec{a}|$. The exact solution of (9) can be written as

$$\overline{\mathbf{U}}(t') = \sum_{j=1}^{N^{CV,tot}} C_j^0 \mathbf{V}_j \exp\left[\lambda_j t'\right], \tag{10}$$

with λ_j and $\mathbf{V}_j$ the eigenvalues and eigenvectors of the matrix $\mathbf{M}$, and the coefficients C_j^0 are defined by the initial solution, such that

$$\overline{\mathbf{U}}(0) = \sum_{j=1}^{N^{CV,tot}} C_j^0 \mathbf{V}_j. \tag{11}$$

For the solution to be stable, all the eigenvalues λ_j should have a non-positive real component, since a positive real component would lead to an exponentially growing, and thus unstable, mode.

5. Results of stability analysis

For all the results given in this section, N^{GP} was set to 13, which yields a mesh with $N^{SV} = 130$ cells. With the second-order scheme, there are then $N^{CV,tot} = 520$ CV-averaged solutions on the mesh, and $N^{CV,tot} = 1300$ with a third-order scheme.

5.1. Second-order scheme

This scheme is stable for the problem described in the previous section. The eigenvalues of the matrix M are plotted in Fig. 5. The stability of this scheme was also verified for meshes with more cells.

5.2. Two-parameter family of partitions for the third-order scheme

Here, the family of third-order partitions shown in Fig. 2(a) is considered. Fig. 6 shows the logarithm in base ten of the maximum real eigenvalue λ_{Re}^{max} obtained with the stability analysis, for α varying between 1/20 and 1/2 with steps of 1/20 and β between 2/30 and 2/3 with steps of 2/30. Notice that the additional boundary imposed by $\beta \leqslant 4\alpha/(4\alpha+1)$ has also been plotted in this figure. For the scheme to be stable, λ_{Re}^{max} should be zero, and thus the logarithm should be minus infinity.

Fig. 7 shows three plots where λ_{Re}^{max} is plotted versus α and β in more detail, in a zone where λ_{Re}^{max} is small. It is seen that in these zones, there are no steep gradients in the evolution of λ_{Re}^{max} as a function of α and β, and it is expected that the resolution in α and β is enough to get a clear picture of the evolution of λ_{Re}^{max}. The maximum real eigenvalue is never below $1e-3$, meaning that none of the partitions yields a stable scheme.

5.3. Three-parameter families of partitions for the third-order scheme

For the three-parameter third-order partition families shown in Figs.2(b), 3(a) and (b), the stability analysis yields similar results as for the two-parameter family in the previous section. The evolution of λ_{Re}^{max} versus α, β and γ for these partition families has been plotted in Figs. 8–10, respectively. The maximum real eigenvalue is never below $1e-3$, indicating that there is again no partition that yields a stable scheme.

6. Test case

To verify the theoretical results presented in the previous section, the test problem used for the stability analysis was solved with the second-order SV scheme and two third-order SV schemes. The first third-order scheme was proposed by Chen [9] and is defined by $\alpha = 0.1093621117, \beta = 0.1730022492$ and γ given by (6). The other third-order scheme was proposed in Liu et al. [6] and corresponds to $\alpha = \beta = \gamma = 0.25$. Both schemes belong to the first family of third-order partitions that were discussed above. The same configuration as described above was used for this problem, with the cell size Δx equal to 1.0. The initial solution was a plane wave with a Gaussian profile, given by

$$u(x,y,z,t=0) = \exp\left[-\left(\frac{x-2.5}{0.5}\right)^2\right]. \tag{12}$$

For the integration in time, the third-order total variation diminishing Runge–Kutta (TVD R–K) scheme (see [16]) was used, with a time step equal to 0.01. The magnitude of the propagation speed $|\vec{a}|$ was set to one, which results in a CFL number equal to 0.01. The residual histories are plotted in Fig. 11. As predicted by the analysis, the second-order scheme is stable, while the third-order schemes are not.

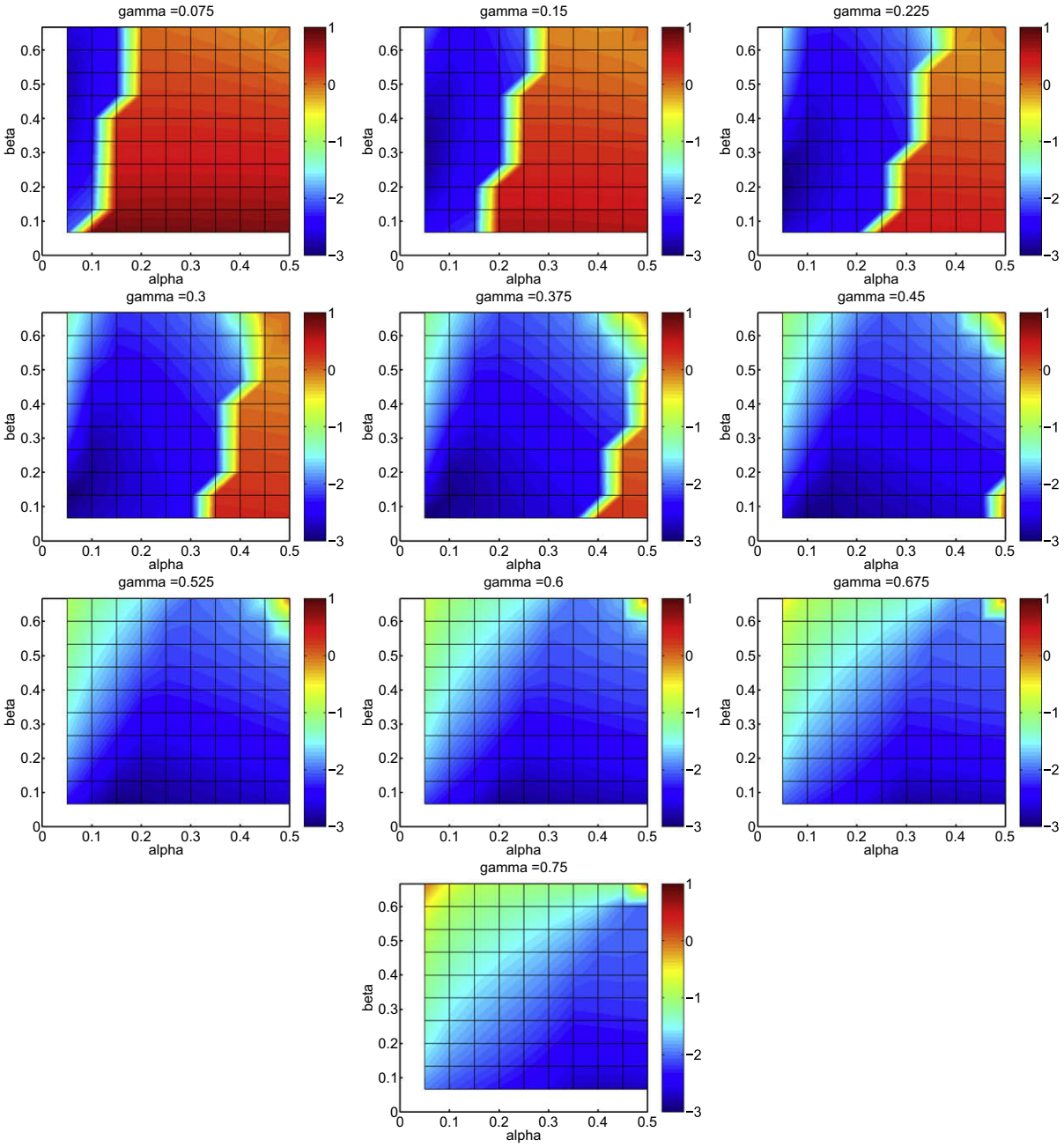

Fig. 10. Logarithm in base ten of maximum real eigenvalue of the matrix **M** for the third three-parameter family of third-order partitions, for partition parameters $\alpha = \frac{1}{20} + l\frac{1}{20}, \beta = \frac{2}{30} + m\frac{2}{30}$ and $\gamma = \frac{3}{40} + n\frac{3}{40}$, with $l, m, n = 0, \ldots, 9$.

7. Conclusions

In the present note, the stability of second- and third-order spectral volume schemes for 3D tetrahedral grids has been analyzed. The matrix method for stability analysis was applied on a model problem, namely a linear advection along the axial direction of a long periodic channel. This model problem allows to detect weak instabilities in solution modes with a long wavelength with respect to the cell size. With this stability analysis, it was confirmed that the second-order scheme is stable. However, no stable schemes were found in a two-parameter family of third-order SV partitions that has previously been considered in literature. An effort was made to achieve a stable scheme by considering three more general three-parameter families of partitions, but the effort was not successful. New ideas are needed to stabilize the 3D third-order SV schemes for

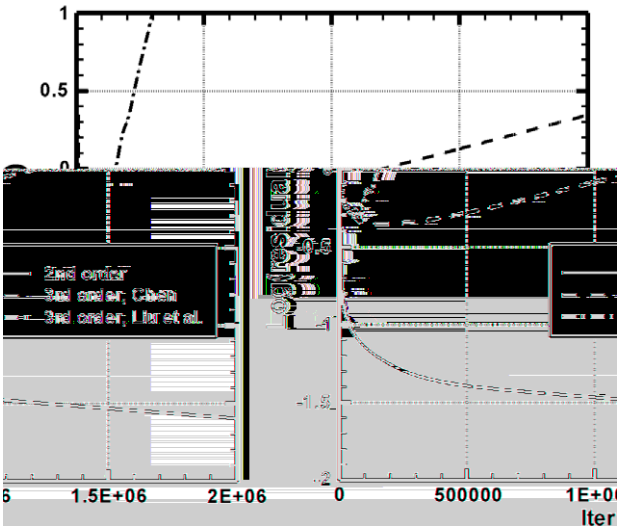

Fig. 11. Comparison of residual histories for 3D linear advection model problem.

tetrahedral grids. As a test, the model problem used for the analysis was solved numerically with second- and third-order SV schemes. The results of this test were in agreement with those of the analysis.

Acknowledgment

Part of this research was funded by IWT under Project No. SBO 050163. This funding is gratefully acknowledged.

References

[1] Zhi Jian Wang, Spectral (finite) volume method for conservation laws on unstructured grids: basic formulation, J. Comput. Phys. 178 (2002) 210–251.
[2] Zhi Jian Wang, Yen Liu, Spectral (finite) volume method for conservation laws on unstructured grids II: extension to two-dimensional scalar equation, J. Comput. Phys. 179 (2002) 665–697.
[3] Zhi Jian Wang, Yen Liu, Spectral (finite) volume method for conservation laws on unstructured grids III: one dimensional systems and partition optimization, J. Sci. Comput. 20 (2004) 137–157.
[4] Zhi Jian Wang, L. Zhang, Yen Liu, Spectral (finite) volume method for conservation laws on unstructured grids IV: extension to two-dimensional Euler equations, J. Comput. Phys. 194 (2) (2004) 716–741.
[5] Zhi Jian Wang, Yen Liu, Extension of the spectral volume method to high-order boundary representation, J. Comput. Phys. 211 (2006) 154–178.
[6] Yen Liu, Marcel Vinokur, Zhi Jian Wang, Spectral (finite) volume method for conservation laws on unstructured grids V: extension to three-dimensional systems, J. Comput. Phys. 212 (2006) 454–472.
[7] Yuhzi Sun, Zhi Jian Wang, Yen Liu, Spectral (finite) volume method for conservation laws on unstructured grids VI: extension to viscous flow, J. Comput. Phys. 215 (2006) 41–58.
[8] Rob Harris, Zhi Jian Wang, Yen Liu, Efficient quadrature-free high-order spectral volume method on unstructured grids: theory and two-dimensional implementation, J. Comput. Phys. 227 (2008) 1620–1642.
[9] Qian-Yong Chen, Partitions of a simplex leading to accurate spectral (finite) volume reconstruction, SIAM J. Sci. Comput. 27 (4) (2006) 1458–1470.
[10] Bernardo Cockburn, Chi-Wang Shu, TVB Runge–Kutta local projection discontinuous Galerkin finite element method for conservation laws V: multidimensional systems, J. Comput. Phys. 141 (1998) 199–224.
[11] Yuhzi Sun, Zhi Jian Wang, Yen Liu, High-order multidomain spectral difference method for the Navier–Stokes equations on unstructured hexahedral grids, Commun. Comput. Phys. 2 (2) (2007) 310–333.
[12] Kris Van den Abeele, Chris Lacor, Zhi Jian Wang, On the connection between the spectral volume and the spectral difference method, J. Comput. Phys. 227 (2) (2007) 877–885.
[13] Kris Van den Abeele, Tim Broeckhoven, Chris Lacor, Dispersion and dissipation properties of the 1D spectral volume method and application to a *p*-multigrid algorithm, J. Comput. Phys. 224 (2) (2007) 616–636.
[14] Kris Van den Abeele, Chris Lacor, An accuracy and stability study of the 2D spectral volume method, J. Comput. Phys. 226 (1) (2007) 1007–1026.
[15] C. Hirsch, Numerical Computation Internal and External Flows. Fundamentals of Numerical Discretization, vol. 1, John Wiley & Sons, Chichester, New York, Brisbane, Toronto, Singapore, 1988.
[16] Chi-Wang Shu, Total variation diminishing Runge–Kutta schemes, SIAM J. Sci. Stat. Comput. 9 (1988) 1079–1084.